Geomechanical Analysis of Pressure Limits for Thin Bedded Salt Caverns

by

Michael S. Bruno and Maurice B. Dusseault

Terralog Technologies USA, Inc.
Arcadia, California 91006 USA
(626) 305-8460; www.terralog.com

Spring 2002 Meeting
April 29-30, 2002
Banff, Alberta

Solution Mining Research Institute, Spring 2002 Technical Meeting
Banff, Alberta, Canada, April 29-30

Geomechanical Analysis of Pressure Limits For Thin Bedded Salt Caverns

Michael S. Bruno and Maurice B. Dusseault
Terralog Technologies USA, Inc.
332 E. Foothill Blvd, Arcadia CA, 91006 USA

ABSTRACT

Bedded salt formations are layered and interspersed with non-salt sedimentary materials such as anhydrite, shale, dolomite, and limestone. The "salt" layers themselves also often contain significant impurities. In comparison to relatively homogeneous salt domes, therefore, bedded salt cavern development and operations present additional engineering challenges related to the layered, heterogeneous lithology, differential deformation and bedding plane slip between individual layers, and larger lateral to vertical cavern dimensions.

This paper summarizes results from a recently concluded research project sponsored by the Gas Research Institute. The project effort included a geologic and geomechanical review of three major bedded salt basins in North America (the Permian Basin, the Michigan Basin, and the Appalachian Basins). We evaluated the geologic settings for these bedded salt deposits, and we reviewed geomechanical aspects for typical lithologies encountered. Given that background and insight, we next investigated analytical and numerical methods to estimate the geomechanical response of caverns in such settings to pressure cycling.

The primary limit on maximum cavern pressure is the fracturing pressure for the weakest lithology encountered by the cavern. We present analytical equations describing the influence of heterogeneous bedding layers on stresses in the subsurface. Varying mechanical properties will lead to varying horizontal stress, and hence varying fracture pressure. We illustrate this process with 3D geomechanical models of caverns in bedded salt.

A second potential constraint on gas storage operations is the pressures at which bedding plane slip or mechanical damage may be induced in heterogeneous layers surrounding the cavern or in the overburden. Bedding plane slip at the cavern boundary can lead to lateral gas migration, while bedding plane slip in the roof and caprock can lead to well damage and to roof caving. We present a theoretical review of stresses induced by pressure cycling, and analytical and 3D geomechanical modeling of various cavern configurations to illustrate the pattern and magnitudes of shear stresses induced around varying geometries. Parametric simulations are presented to illustrate the relative influences of cavern height to diameter ratio, non-salt interbed number and thickness, and salt and non-salt roof-beam thickness on cavern deformation and bedding plane slip.

1. INTRODUCTION AND BACKGROUND

Bedded salt formations are found in several areas throughout the United States and Canada, providing a useful means for storing gas near major markets (see Figure 1). The largest basins include the Permian Basin across Texas, Oklahoma, Kansas, Colorado, and New Mexico, the Gulf

Coast Basin across Southern Texas, Louisiana, Mississippi, and Alabama, and the Michigan and Appalachian Basins across the states of Michigan, Ohio, Pennsylvania and New York. These areas have experienced different deposition and tectonic history, resulting in some differences in depth, lithology and typical geologic structure for the dominant bedded salt intervals.

Bedded salt formations in all areas, however, are layered and interspersed with non-salt sedimentary materials such as anhydrite, shale, dolomite, and limestone. The "salt" layers themselves also often contain significant impurities. In comparison to relatively homogeneous salt domes, therefore, cavern development and operations present additional engineering challenges related to:

- The layered, heterogeneous lithology;
- Differential deformation, creep, and bedding plane slip between individual layers;
- Somewhat larger lateral to vertical cavern dimensions;

Several organizations have developed guidance documents for designing and operating storage salt caverns (CSA 1993; API 1994; IOGCC 1995). Few of these efforts, however, have focused on some of the critical technical aspects related to cavern development in thin, heterogeneous, bedded salt formations.

There are three basic geomechanical processes that limit maximum and minimum pressures in a bedded salt cavern. These are:

1. The tensile fracturing pressure for the salt material and interbedded non-salt materials;
2. The formation stresses, induced by cavern pressure decline or increase, at which bedding plane slip might be induced between heterogeneous material layers;
3. The minimum cavern pressure that might induce roof instability or excessive closure.

The goals of this project, sponsored by the Gas Research Institute, have been to investigate and summarize for operators each of these limiting factors, and to present guidelines and analysis tools to determine minimum and maximum pressure limits for bedded salt caverns in a variety of structural settings.

Due to tectonic deformation and structural effects, the regional state of stress in the deep subsurface is generally non-hydrostatic. That is, horizontal stresses are generally non-uniform and unequal to the vertical lithostatic stress. In relatively homogeneous salt domes, the viscoelastic salt material creeps over geologic time and redistributes this regional stress loading into a more uniform stress condition nearly equal to the overburden load (lithostatic stress). This results in a uniform and relatively high fracture pressure for all of the salt material surrounding a salt dome cavern.

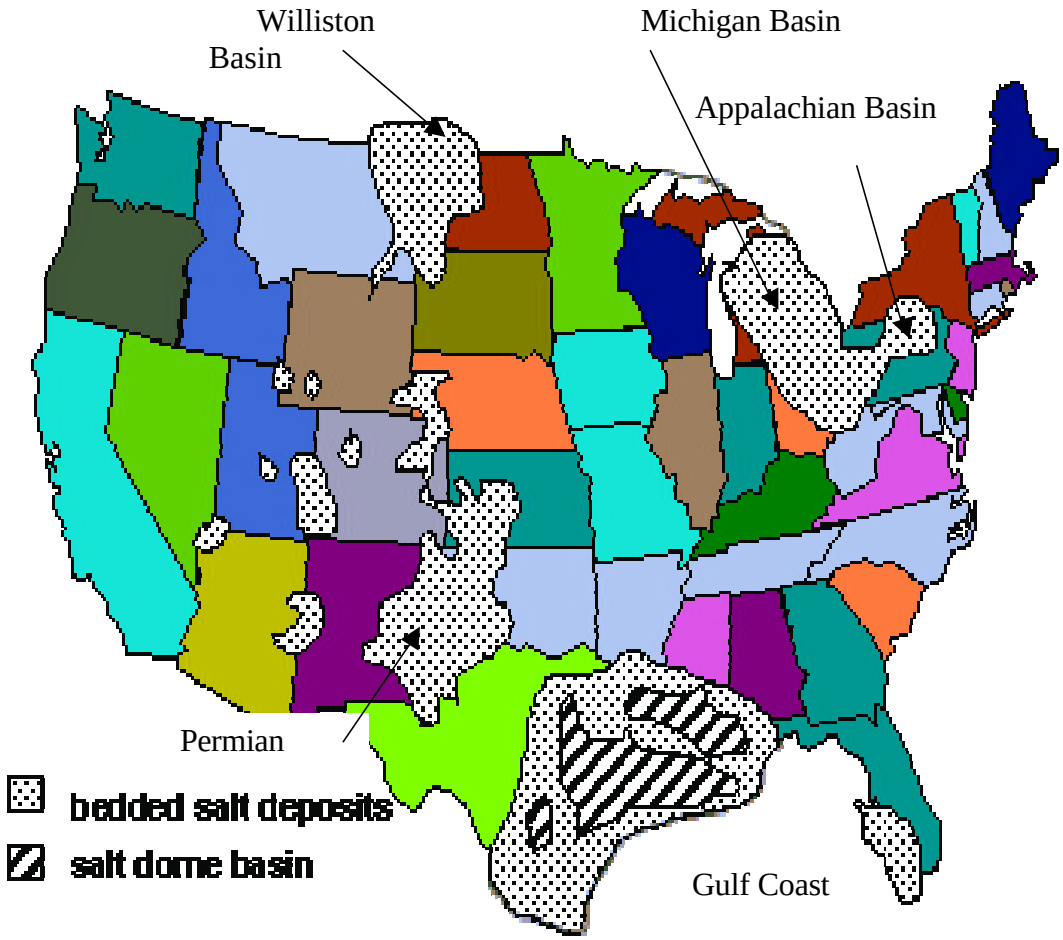

Source: National Petroleum Technology Office

Figure 1. Bedded Salt Deposits in US

Such is not always the case, however, with caverns developed in bedded salt formations. Some non-salt interbedded materials, such as dolomite for example, can sustain significant shear stresses over geologic time. As illustrated in Figure 2, relatively stiff and brittle materials deform and fail in a fundamentally different manner than materials such as salt that creep over time. The result is that different lithology horizons will react differently to far-field loading, leading to different horizontal stresses and associated fracture pressure.

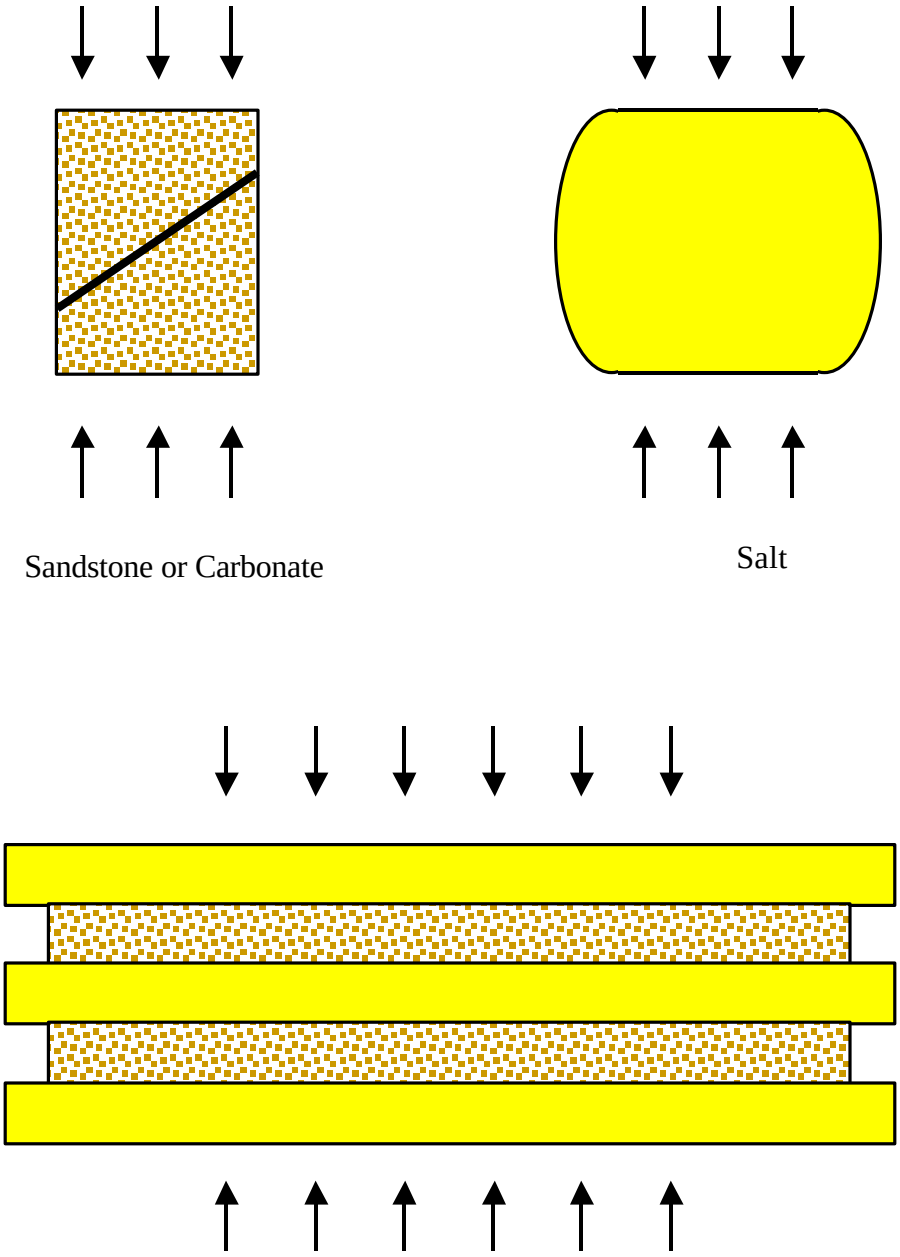

Figure 2. Deformation differences between stiff rock and soft evaporates

One objective of this project, therefore, has been to investigate and summarize fracture pressure variations in heterogeneous material layers and provide guidelines for recognizing when this might occur and how to take this into consideration in design and operations. The effort has included review and documentation of available literature and field data in the three primary basins, analytical and numerical modeling of composite layers for illustrative purposes, and documentation of a step-by-step evaluation methodology for operators.

A second potential constraint on gas storage operations is the pressure at which bedding plane slip or mechanical damage may be induced in heterogeneous layers surrounding the cavern or in the overburden due to pressure cycling in the storage interval. This bedding plane slip can be induced by two mechanisms. In the first type of process pore pressure increase between lithology boundaries may relieve the normal stress sufficiently to allow existing shear stresses to activate the plane. In the second type of process cavern compaction during pressure decline and cavern dilation during pressure increase can produce shear stresses of sufficient magnitude to induce slip on bedding planes or create new faults. Bedding plane slip adjacent to caverns can lead to lateral gas migration, while bedding plane slip in the roof and overburden areas can lead to well damage.

The pattern and magnitude of stresses induced by pressure cycling can be evaluated with geomechanical models and compared with measured or estimated lithology interface properties. A second objective of this project, therefore, has been to investigate and summarize the geomechanical processes and to provide guidelines and numerical tools to evaluate the influence of pressure cycling on heterogeneous layers in the caprock and confining materials. This effort has also included a theoretical review and summary of stresses induced by pressure cycling, analytical and numerical modeling of various cavern configurations to illustrate the pattern and magnitudes of shear stresses induced around varying geometries, and development of a step-by-step evaluation methodology for operators.

2. ANALYTICAL DESCRIPTIONS

Due to tectonic deformation and structural effects, the regional state of stress is generally non-hydrostatic. That is, horizontal stresses are generally non-uniform and unequal to the vertical lithostatic stress. In relatively homogeneous salt domes, the viscoelastic salt material creeps over geologic time and redistributes this regional stress loading into a more uniform stress condition nearly equal to the overburden load (lithostatic stress). This results in a uniform and relatively high fracture pressure for all of the salt material surrounding a salt dome cavern. Such is not always the case, however, with caverns developed in bedded salt formations. Some non-salt interbedded materials, such as dolomite for example, can sustain shear stresses over geologic time and, depending on relative bed thickness, will experience different in-situ compressive stress than the surrounding salt material. The fracturing pressure for the interbedded material can therefore vary from the fracture pressure in the surrounding salt.

Since salt creeps over geologic time, a reasonable assumption (consistent with field observations) is that horizontal stresses within the salt will be equal to the vertical stress, increasing with depth due to gravitational loading (increasing overburden weight). In addition to gravity, however, there are often tectonic loads which may increase or decrease the principal horizontal stresses. In non-creeping layers, then, a difference in horizontal stresses will develop, sometimes related to the stiffness properties of the material. The minimum horizontal stress controls fracture pressure in a formation, which will therefore vary slightly between different lithologies.

In addition to gravitational and tectonic loading, we must also consider stress changes induced by solution mining the cavern and by subsequent internal pressure cycles during storage operations. Some of these influences can be estimated analytically. Other influences are more complex, and require numerical modeling techniques.

2.1 Influence of heterogeneous layers on earth stresses

The vertical stress at a point below the surface of the earth, in the absence of local structural effects, is generally related to the weight of overlying sediments. This can be expressed by:

$$\sigma_v \approx \int \rho g \, dz$$

where σ_v is the vertical stress, ρ is the bulk density, g is gravity, and the integral is expressed over the total depth from the surface to the subsurface formation depth z. The vertical stress can be estimated by integrating a bulk density log, and is generally on the order of about 1 psi/ft.

The horizontal stresses in a formation cannot be easily estimated, and it is best to measure these in the field with hydraulic fracture testing techniques. We can, however, consider and discuss the relative influence of layering on horizontal stresses by considering various assumed horizontal stress models. The simplest horizontal stress model, for example, is one in which there are no tectonic loads and no lateral strain conditions, such that the horizontal stresses are simply related to the vertical stress through the Poisson effect.

2.2 Stress due to gravitational loads; no-lateral strain conditions

The condition described above is represented by uniaxial strain conditions where the principal vertical and horizontal stresses are related by

$$\sigma_h = \frac{\nu}{(1-\nu)} \sigma_v = \frac{\nu}{(1-\nu)} \int \rho g \mathrm{d}z \, .$$

Then for a layered media neglecting interface effects, the horizontal stresses in different layers (say layer 1 and layer 2) are related to the vertical stress at that depth by

$$\sigma_{h1} = \frac{\nu_1}{(1-\nu_1)} \int \rho g \mathrm{d}z \, ,$$

$$\sigma_{h2} = \frac{\nu_2}{(1-\nu_2)} \int \rho g \mathrm{d}z \, .$$

In this type of relaxed, non-tectonic setting, horizontal stresses and related fracture pressure will therefore increase with higher Poisson's ratio and decrease with lower Poisson's ratio (note that the Poisson ratio ν is always between 0 and 0.5).

2.3 Stress due to gravitational loads plus lateral tectonic strains

Another type of earth model is one in which the horizontal stress is related to the cumulative influence of gravitational loading plus additional tectonic related horizontal strains. In this situation the horizontal stresses are anisotropic (unequal in the horizontal plane) and are given below,

$$\sigma_{h1} = \frac{E}{1-\nu^2}(\varepsilon_{h1} + \nu\varepsilon_{h2}) + \frac{\nu}{(1-\nu)}\int \rho g \, dz ,$$

$$\sigma_{h2} = \frac{E}{1-\nu^2}(\varepsilon_{h2} + \nu\varepsilon_{h1}) + \frac{\nu}{(1-\nu)}\int \rho g \, dz .$$

As before, the horizontal stresses and the related fracture pressure increase with the Poisson ratio. In this situation, however, they are also influenced by the Young's Modulus, E, of the material. This parameter generally varies to a larger extent than Poisson's Ratio, and in many cases will have the more dominant influence on stress and fracture pressure.

2.4 Influence of layering on fracture stresses around a cavity

Next we discuss the general influence of layering on fracture stresses around a cylindrical cavity. As a first approximation we neglect the boundary effects at the cavern roof and base, and consider only elastic stresses near the center height of the cavity. For each material layer, we consider a horizontal plane with a circular opening and prescribed boundary conditions at infinity and at the cavity surface. Let the horizontal boundary condition at infinity be given by tectonic pressures σ_{h1} and σ_{h2} directed along two perpendicular directions and assume a constant internal pressure p applied to the surface of the cylindrical cavity. If the radius of the cylindrical cavity is R, this boundary conditions read $\sigma_r = p$ for r = R. The previous solution for σ_{h1} and σ_{h2} can now be used as an estimate for the horizontal stresses σ_1 and σ_2.

The horizontal stress components are now given by the radial stress component

$$\sigma_r = \frac{1}{2}(\sigma_1 + \sigma_2)(1 - \frac{R^2}{r^2}) + \frac{pR^2}{r^2} + \frac{1}{2}(\sigma_1 - \sigma_2)(1 - \frac{4R^2}{r^2} + \frac{3R^4}{r^4})\cos 2\theta ,$$

and by the tangential normal stress

$$\sigma_\theta = \frac{1}{2}(\sigma_1 + \sigma_2)(1 + \frac{R^2}{r^2}) - \frac{pR^2}{r^2} - \frac{1}{2}(\sigma_1 - \sigma_2)(1 + \frac{3R^4}{r^4})\cos 2\theta .$$

If the two perpendicular applied pressures σ_1 and σ_2 are not equal, then in addition to the normal stress components a shear stress develops as well,

$$\tau_{r\theta} = -\frac{1}{2}(\sigma_1 - \sigma_2)(1 + \frac{2R^2}{r^2} - \frac{3R^4}{r^4})\sin 2\theta .$$

The radial displacement at the surface of the cavity is given by

$$\frac{u_R}{R} = \frac{\Delta R}{R} = \frac{1}{E}\left\{\sigma_1 + \sigma_2 - \nu\sigma_3 + 2(1-\nu^2)(\sigma_1 - \sigma_2)\cos 2\theta - p(1+\nu)\right\}$$

where p is the pressure in the cavity and σ_3 is the stress in the vertical direction.

The tangential normal stress controls hydraulic fracture pressure. The implications of the solution described above, therefore, is that the maximum safe pressure in the cavern will again depend on the elastic properties of individual layers (through their influences on horizontal stresses). If minimum horizontal stresses and fracture pressure are estimated from the analytical solutions provided above, they should be compared with the minimum far-field horizontal stresses and the lower value used to estimate minimum fracture pressure in any given lithology.

2.5 Some influences of layering on roof deformation and stability

To obtain some guidance on the influences of layering on roof deformation and stability, we can start with simple composite beam theory to estimate maximum tensile and shear stress components. We assume that the failure of the beam in bending is determined by the tensile strength of the material. Consider a composite roof beam comprised of two materials characterized by the mechanical constants E_1 and E_2 and by their thickness h_1 and h_2 as shown in Figure 3 below.

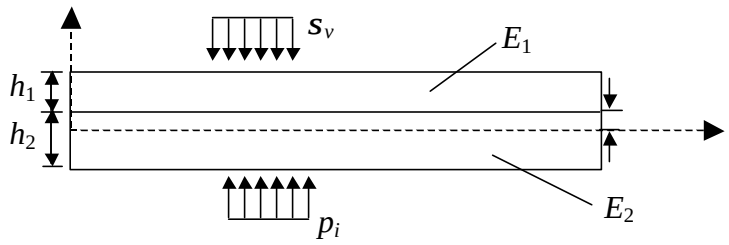

Figure 3. Neutral axis for composite roof beam depends on layer stiffness properties

The applied load to the upper surface of the roof beam is given by the vertical stress σ_v and the applied load to the lowermost surface is given by the cavity pressure p_i. Therefore, the total applied load is equal to (σ_v - p_i). Varying end conditions can be considered, but a fixed-fixed end condition might be most suitable for an approximate analytical solution. Internal cavern pressure is always less than the vertical stress, so that the roof beam always sags downward into the cavern.

For standard beam theory, the normal force N must vanish for any transversely applied load, so that the location of the neutral axis can be determined as:

$$h = \frac{E_2 h_2^2 - E_1 h_1^2}{2E_2 h_2 + 2E_1 h_1}.$$

From the normal stress distribution $\sigma_x = -Eyv''$, where *y* is the distance from the neutral axis, the bending moment can be determined by integration over the cross-sectional area *A*, such that

$$M = -\frac{v''}{3}\left\{E_2\left[h^3 - (h_2 - h)^3\right] + E_1\left[(h_1 + h)^3 - h^3\right]\right\}.$$

The bending moment is also related to the applied distributed load *q*

$$\frac{d^2M}{dx^2} = -q\,,$$

where the applied load *q* is given by $\sigma_v - p_i$. Integrating this last equation provides two constants of integration, which may be used to impose proper boundary condition,

$$M_{(x)} = -q\frac{x^2}{2} + C_1 x + C_2\,.$$

For a simple supported beam, the boundary conditions C_1 and C_2 become

$$C_1 = \frac{ql}{2}, \quad C_2 = 0$$

and the curvature of the beam is

$$v'' = \frac{d^2v}{dx^2} = \frac{3}{2}\left\{\frac{q(lx - x^2)}{E_2\left(h^3 - (h_2 - h)^3\right) + E_1\left((h_1 + h)^3 - h^3\right)}\right\}.$$

From the known curvature, the maximum bending stresses can be easily be determined and compared to minimum horizontal stresses in the formation,

$$\sigma_{layer1} = -E_1 yv'', \quad \sigma_{layer2} = -E_2 yv''\,.$$

For a fixed-fixed beam, the constants C_1 and C_2 can be determined as

$$C_1 = \frac{ql}{2}, \quad C_2 = -\frac{ql^2}{12},$$

and the curvature changes to

$$v'' = \frac{d^2v}{dx^2} = \frac{3}{2}\left\{\frac{q\left(lx - x^2 - \frac{l^2}{6}\right)}{E_2\left(h^3 - \left(h_2 - h\right)^3\right) + E_1\left(\left(h_1 + h\right)^3 - h^3\right)}\right\}.$$

Given the new curvature, the maximum tensile stresses can be determined using the same expressions as before.

What are the implications of this analytical approximation? We note that the roof beam curvature and stresses are dependent on both the material properties of the composite layers and on the thickness of these individual layers. The equations listed above can be used to compare the relative stresses and fracture risks developed for alternative composite roof configurations. For roof beams of greater complexity than a couple layers, however, the analytical solutions become quite complex and it is more practical to pursue numerical modeling.

3. NUMERICAL INVESTIGATIONS

3.1 Simulation Matrix and Model Description

For this project Terralog developed a set of three dimensional geomechanical models to investigate cavern deformation and bedding plane slip for a variety of cavern configurations. The Cavern Model Program is illustrated in Figure 4. A windows based graphical interface was developed to specify varying lithology layers (number, depth, thickness) and varying cavern geometry parameters (depth, height, radius). Interfaces between layers of differerent lithology provide potential slip planes, controlled by induced shear stresses, normal stress, and friction properties.

Table 1 summarizes the initial set of geomechanical models developed for this project. The baseline configuration (simulation model 1) is a cylindrical shaped cavern 200m in height and 200m in diameter, with a stepped (roughly spherical) shaped roof as shown in Figure 4. The cavern lies at a depth of about 1400m below the surface. It is assumed to be dissolved in a salt zone that includes one non-salt interbed placed at a central point, and one non-salt interbed placed between the salt roof beam and the overburden material. As summarized in Table 1, the thickness of the non-salt roof beam is varied from 5m to 20m (simulations 1,2,3). The lithology is varied between anhydrite and shale (simulations 1,4). The salt roof beam thickness is varied from 10m to 50m (simulations 1,5,6). The ratio of cavern height to diameter is varied from 0.5 to 2 (simulations 1,7,8). The thickness of the interbed at the center of the salt is varied from 15m to 60m (simulations 1,9,10). And finally, the number of interbeds is varied from 1 to 2 (simulations 1,11).

The simulations performed are sufficient to provide some insight on the relative influence of these few parameter variations. Additional simulations for a wider range of parameter variations are required to confirm and better quantify these observations.

Table 1. Cavern Configuration Simulation Matrix

Simulation Model #	Non-Salt Roof Beam		Salt Roof Beam	Cavern Dimensions		Interbeds			Comments
	Thickness [m]	Material	Thickness [m]	Height/Diameter Ratio	Height [m]	% of Cavern Height	Thickness [m]	Number of Interbeds	
1	10	Anhydrite	20	1	300	10	30	1	Base Line Case
2	5	Anhydrite	20	1	300	10	30	1	Thickness of Non-Salt Roof Beam
3	20	Anhydrite	20	1	300	10	30	1	Thickness of Non-Salt Roof Beam
4	10	Shale	20	1	300	10	30	1	Material of Non-Salt Roof Beam
5	10	Anhydrite	10	1	300	10	30	1	Thickness of Salt Roof Beam
6	10	Anhydrite	50	1	300	10	30	1	Thickness of Salt Roof Beam
7	10	Anhydrite	20	0.5	400	10	40	1	Ratio of Cavern Height/Diameter
8	10	Anhydrite	20	2	500	10	50	1	Ratio of Cavern Height/Diameter
9	10	Anhydrite	20	1	300	5	15	1	Thickness of Interbeds (%)
10	10	Anhydrite	20	1	300	20	60	1	Thickness of Interbeds (%)
11	10	Anhydrite	20	1	300	10	30	2	Number of Interbeds

The geomechanical simulations are performed using Itasca's FLAC3D modeling software. The salt material is modeled using default WIPP creep model parameters. The non-salt material is modeled with Mohr-Coulomb plasticity parameters estimated in our previous geomechanical review. A summary of material properties is presented in Table 2.

Table 2. Material Properties Used in Parametric Simulations

Material	Bulk Modulus [MPa]	Shear Modulus [MPa]	Density [kg/m³]	Tension [MPa]	Cohesion [MPa]	Friction Angle
Anhydrite	74000	25000	3000	7	20	35
Dolomite, Limestone	40000	25000	2700	4	15	35
Shale	13000	8000	2600	1	5	20
Red-beds, Breccias	20000	18000	2000	4	2	35
Salt	50000	10710	2100			

Parameters for the Wipp Model		
A		4.56
B		127
D		5.79E-36 $Pa^{n}s^{-1}$
n		4.9
Q	Activation Energy	12000 cal/mol
R	Universal Gas Constant	1.987 cal/mol K
ε^{*}_{ss}	Steady State Creep Rate	5.39E-08

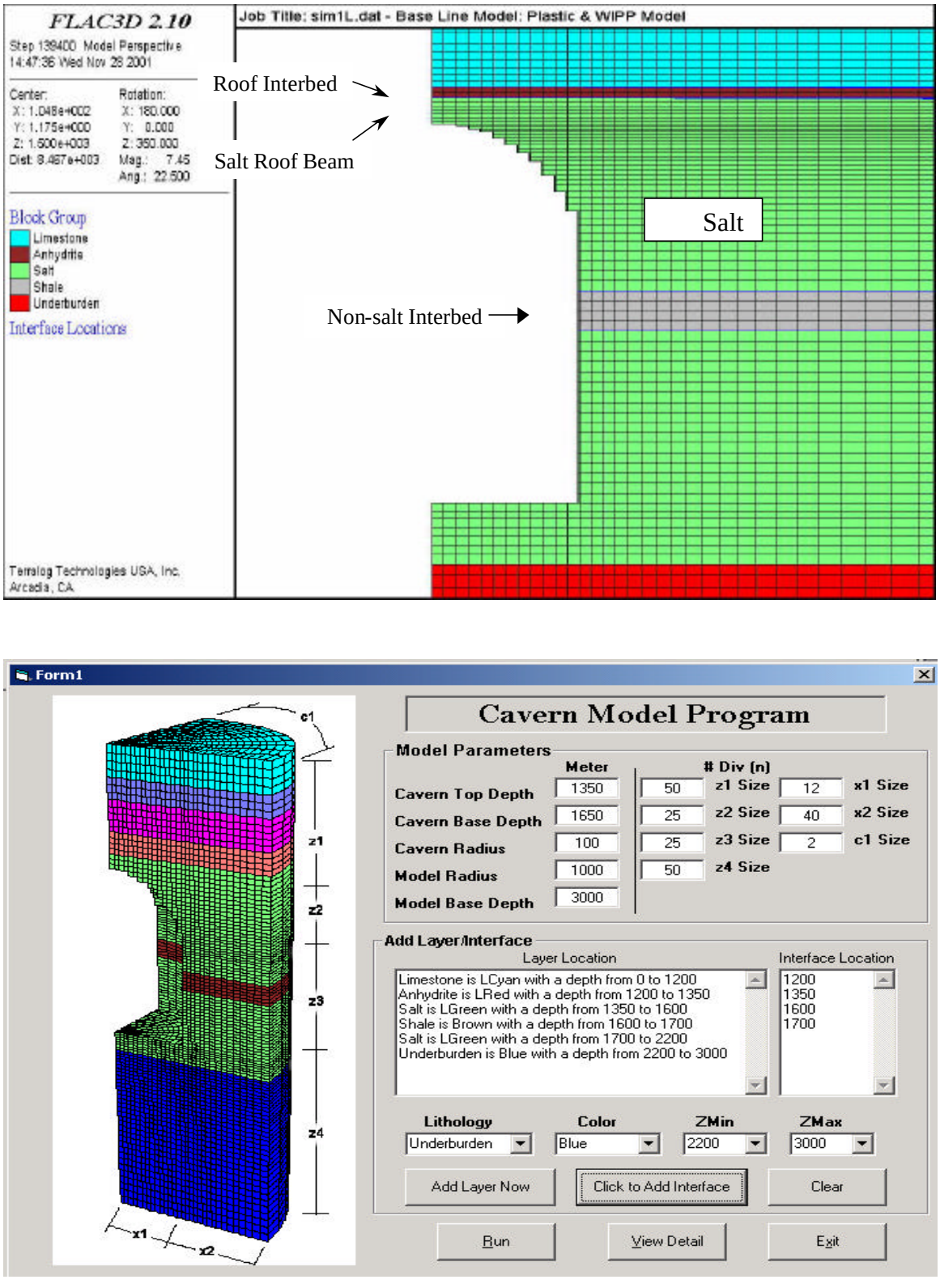

Figure 4. 3D Geomechanical Models for Analyzing Varying Cavern Configurations

For each simulation a vertical stress is developed consistent with the density of overlying sediments (i.e. increasing with depth and equivalent to $s_v \approx \int \rho g \, dz$). Lateral displacements at the outer radius of the model are fixed, so that horizontal stresses develop consistent with the vertical load and the Poisson Ratio for the various lithology layers. The general simulation process may be summarized as follows:

1. Define initial geologic layers and initial stress conditions;
2. Excavate cavern, apply an internal cavern pressure equal to the hydrostatic head of water (about 15MPa at a depth of 1500m);
3. Allow model to run and stresses to creep and equilibrate for 3 months;
4. Impose a 1-year pressure cycle in which cavern pressure increases to 30MPa in 3 months, returns to 15MPa after 6 months, decreases to 0MPa after 9 months, and returns to 15MPa. This is followed by about 30 days of steady state creep and equilibrium.

For each parametric simulation we evaluate roof displacements, cavern sidewall displacements, and bedding plane slip at various lithology interfaces.

3.2 Baseline Simulation Results

Figures 5 and 6 present a summary of deformation vs. time for the top, bottom, and side of the cavern for the baseline simulation. At the end of the pressure cycles roof displacement is on the order 2m and side wall closure is on the order of 3.5m. Displacement and stress contour plots are presented in Figures 7 and 8 for the end of the load cycle.

The horizontal stresses within the interbed near the center of the cavern are lower than the horizontal stresses in the salt, indicating greater risk for hydraulic fracturing during pressure increase. As discussed in the previous section, this is primarily due to the lower Poisson's ratio for the anhydrite interbed relative to the surrounding the salt. The salt creep tends to raise the horizontal stresses closer to vertical stresses, whereas that occurs to a lesser extent in the anhydrite. Not only does this stress difference increase hydraulic fracture risk, but when combined with the stiffness contrast the stress difference also contributes to bedding plane slip risk.

As shown in Figures 7 and 8, both the horizontal displacement contours and the horizontal stress contours are discontinuous across the lithology boundaries at the end of the load cycle, indicating bedding plane slip. Maximum slip on the order of 1.4m occurs at the base of each interbed, primarily during the pressure depletion cycle when cavern pressure drops below hydrostatic levels. Bedding plane slip risk is primarily driven stress differences (rather than absolute magnitude). The difference between cavern pressure and the surrounding rock strength is greatest during pressure depletion, and becomes more equalized during pressurization. Hence the risk for slip is highest during low-pressure cycles.

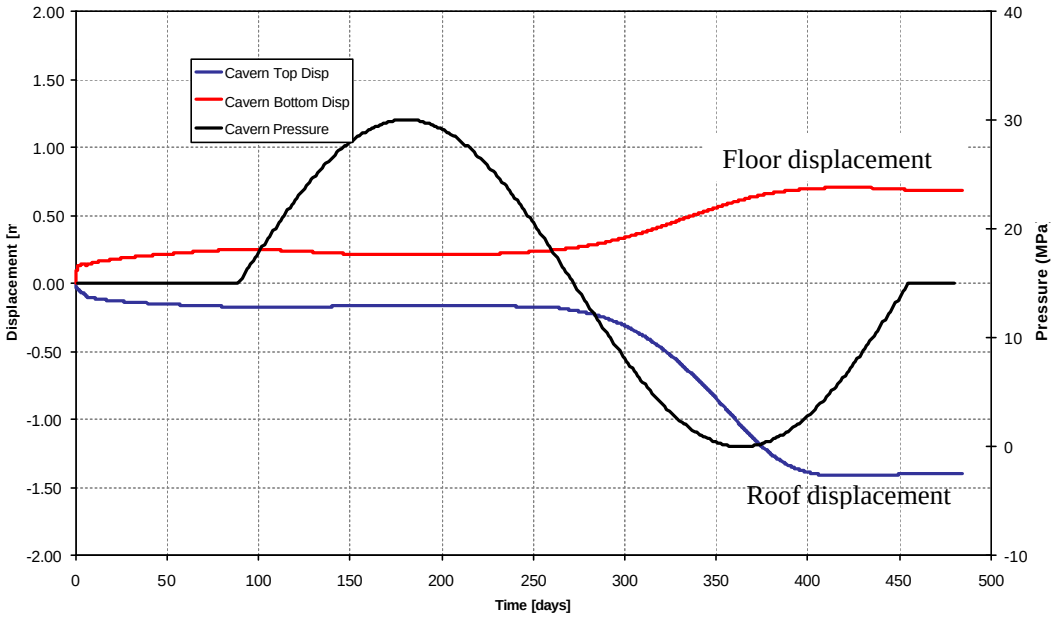

Figure 5. Baseline Simulation Roof and Floor Deformations

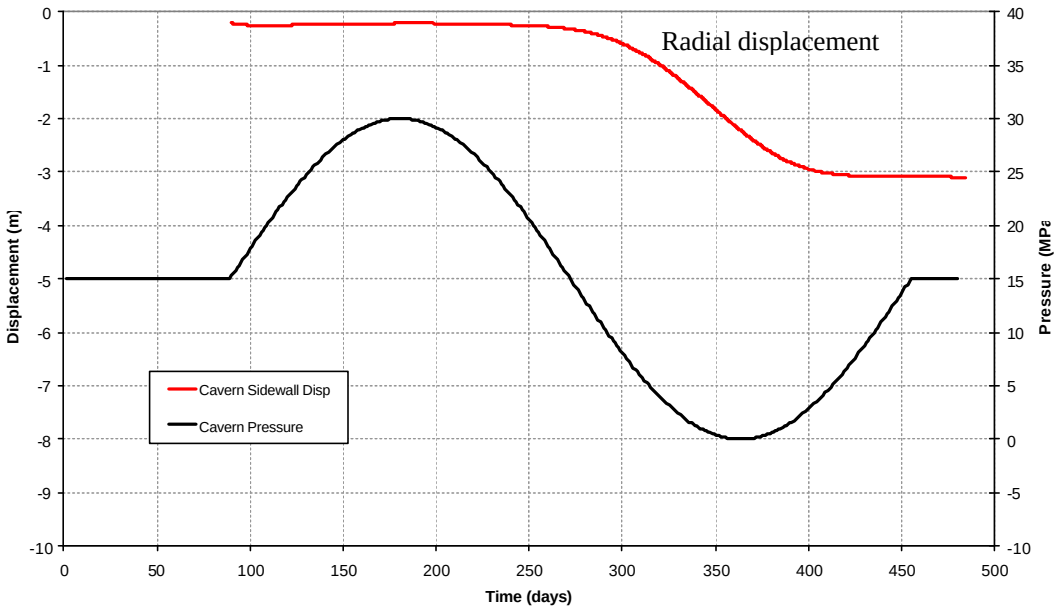

Figure 6. Baseline Simulation Cavern Side Wall Deformation

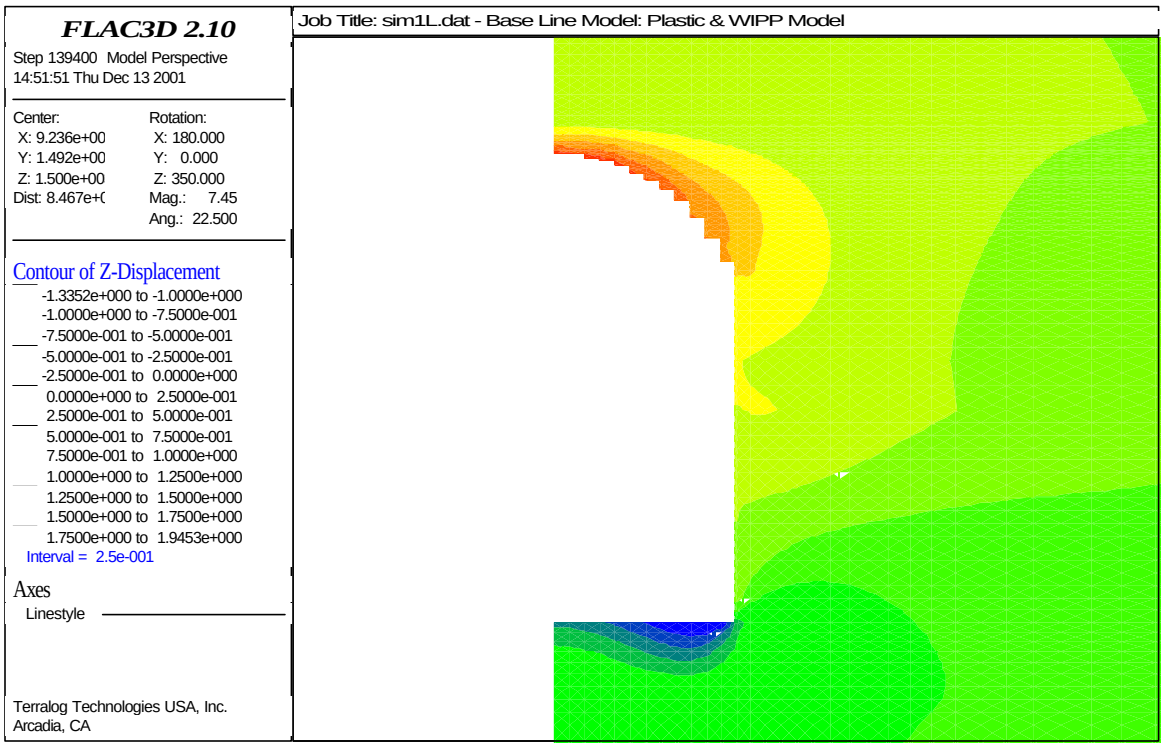

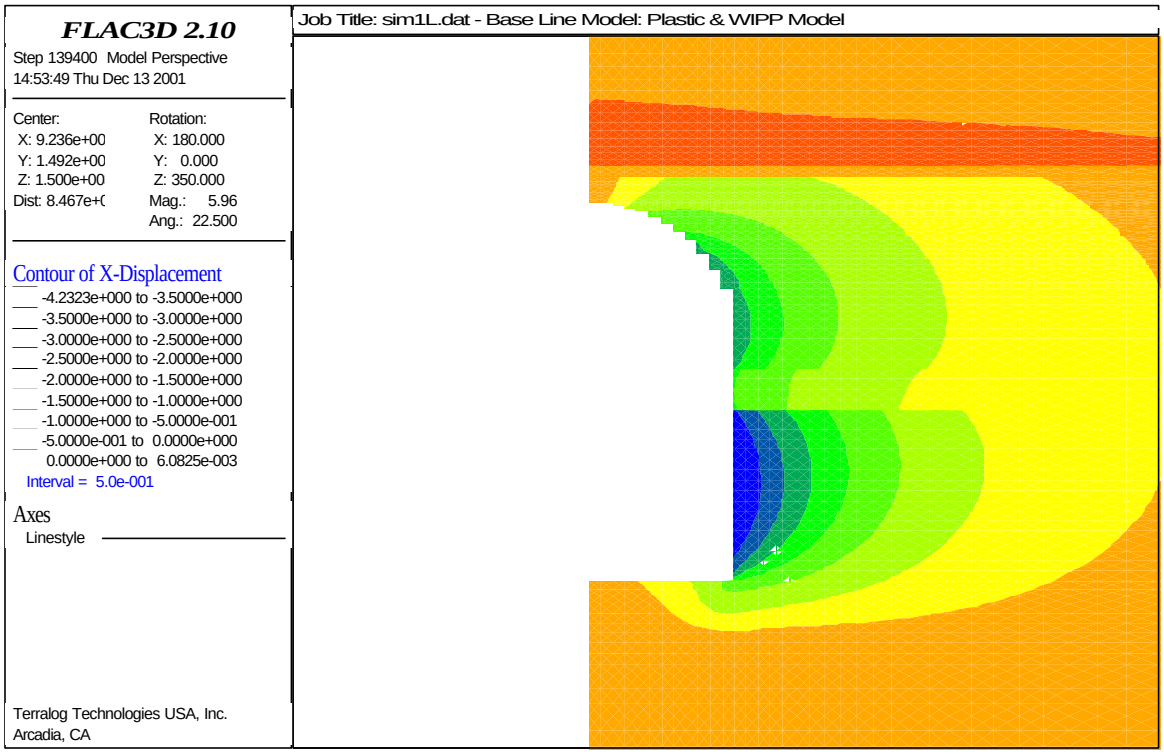

Figure 7. Vertical (upper image) and horizontal (lower image) displacement contours

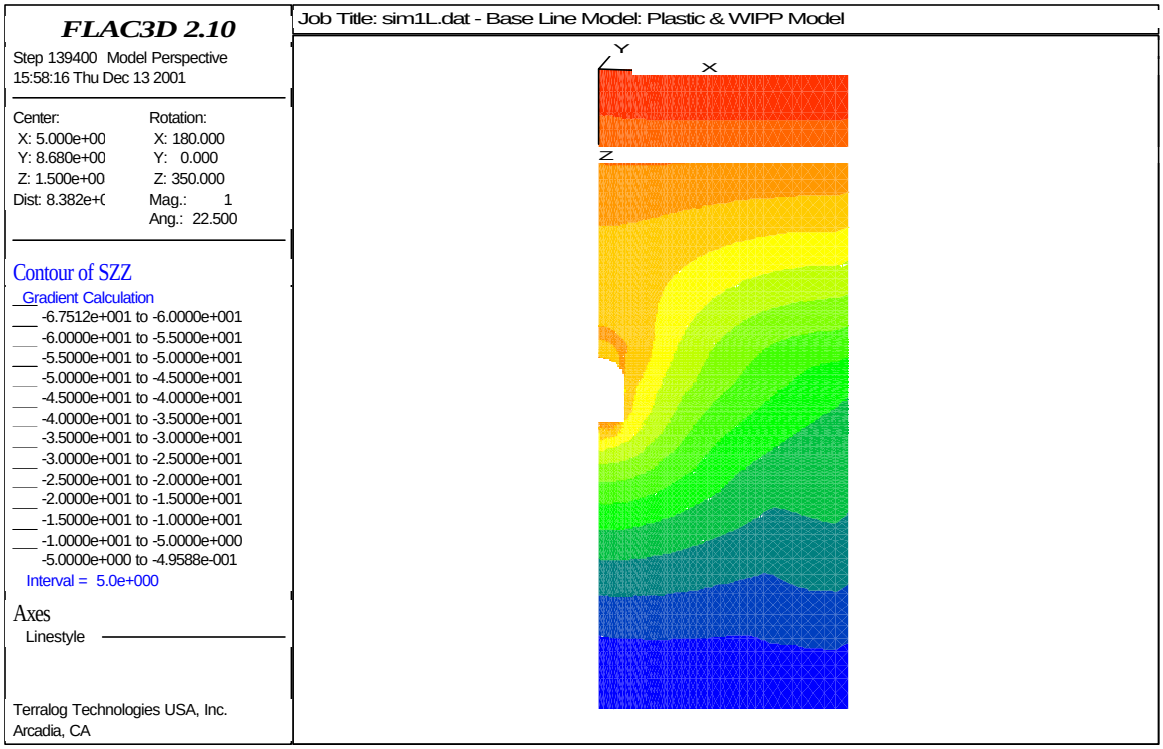

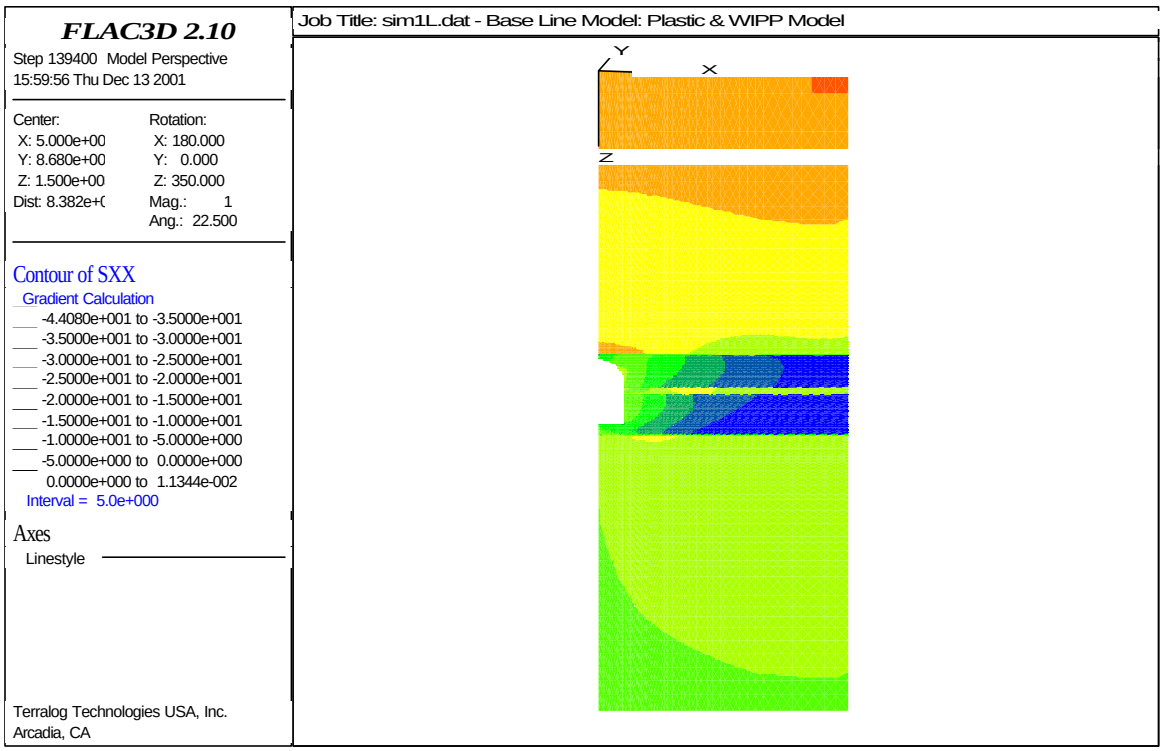

Figure 8. Vertical (upper image) and Horizontal (lower image) stress contours

3.3 Influence of Cavern Height to Diameter Ratio on Deformation and Slip

Figure 9 presents a summary of interbed slip magnitude for varying cavern height to diameter ratios. Referring to Figure 4, interface 1 is the boundary between the roof interbed and the overburden. Interface 2 is the boundary between the roof interbed and the roof salt beam. Interface 3 is boundary between the salt interbed and the upper salt, and interface 4 is the boundary between the salt interbed and the lower salt.

The baseline simulation slip results, for which the cavern height to diameter ratio is one, are presented in the center of Figure 9. This is seen to be the most stable configuration (with respect to bedding plane slip). Either decreasing or increasing the aspect ratio of the cavern contributes to greater bedding plane slip. The lower height to diameter ratio creates particular concerns for slip at the roof interbed. This increases risk for shear damage to wells, especially if the cavern cross section is not symmetric around the injection/production well. Such localized slip and well shear damage has been documented above many gas reservoirs in the petroleum industry. An example caliper image is presented in Figure 10 for a gas reservoir in Southeast Asia (from Bruno, 2001), where localized shear deformation and damage was noted at the interface of a relatively stiff carbonate and sand interval at the top of a producing gas horizon.

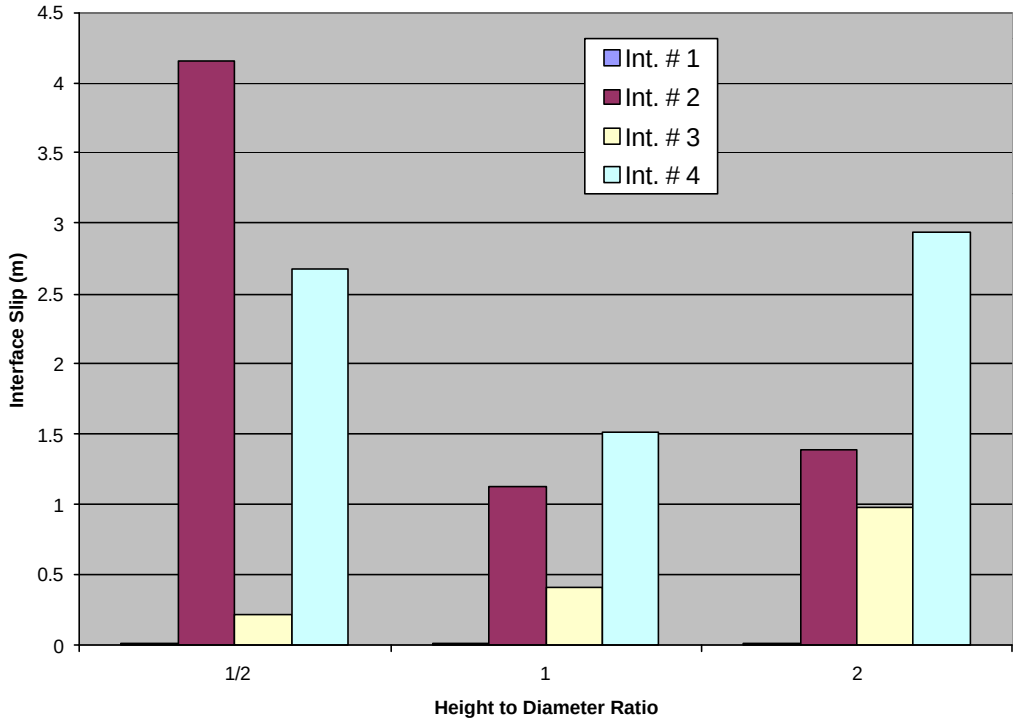

Figure 9. Influence of cavern height to diameter ratio on interface slip

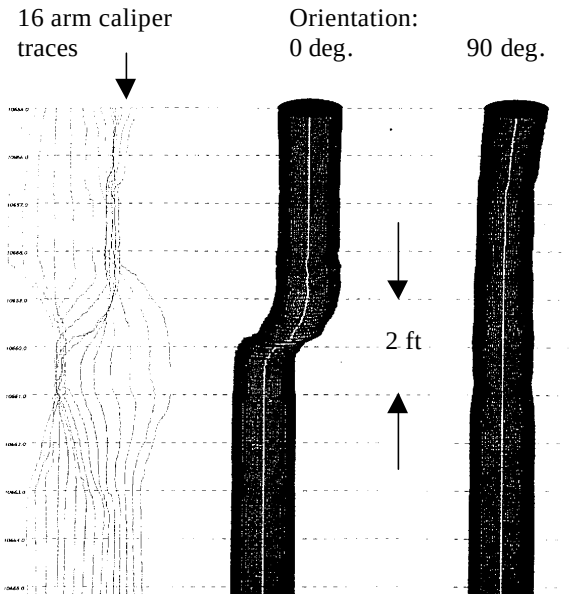

Figure 10. Sample casing deformation pattern noted in caliper logs for damaged gas well in Southeast Asia.

3.4 Influence of Interbeds on Deformation and Slip

Next we investigate the potential influence of interbed variations (number and stiffness) on deformation and slip. Figure 11 compares slip at various interfaces in the roof beam and near the center of the cavern for the baseline simulation in which there is only one central non-salt interbed and another simulation that included two central non-salt interbeds. Again, interface 1 and 2 represent the upper and lower surfaces of the roof interbed. Interface 3 and 4 represent the upper and lower surfaces of the primary central interbed, and interfaces 5 and 6 represent the upper and lower surfaces of the second central interbed.

The additional non-salt interbed near the center of the cavern does not significantly influence the bedding plane slip in the roof interbed or in the first non-salt interbed near the cavern center. It merely seems to provide a location for additional slip. This aspect should be investigated further with additional variations and simulations.

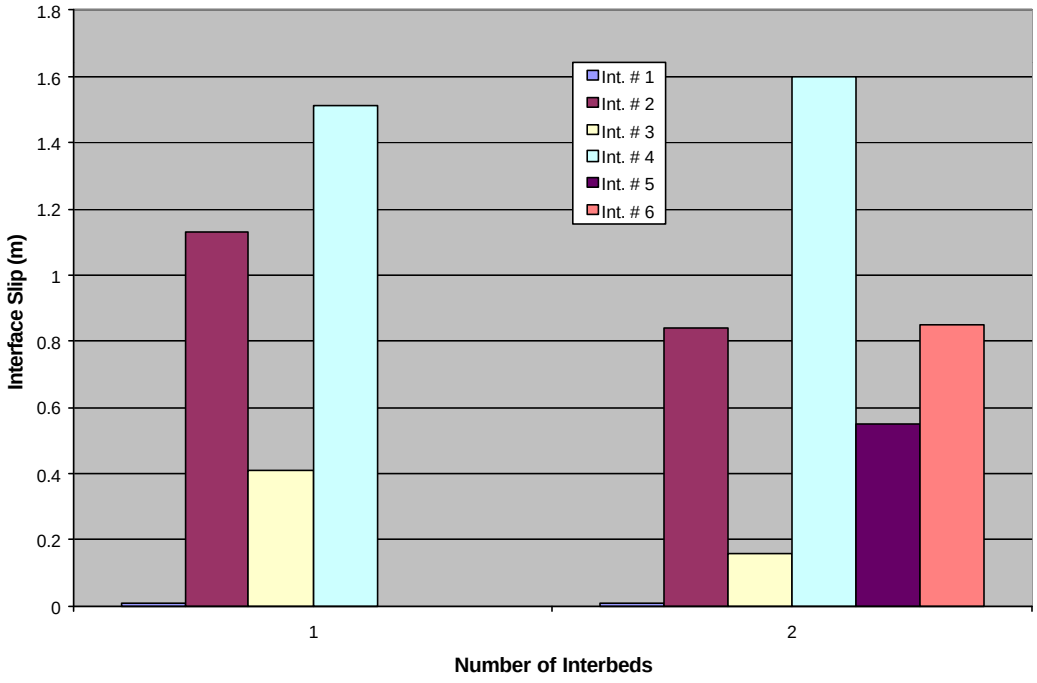

Figure 11. Influence of number of interbeds on interface slip

We also investigated the potential influence of non-salt interbed thickness. The thickness of the central non-salt interbed was varied from 15m to 60m. These simulation results are presented

in Figure 12. There appears to be a consistent trend that increasing interbed thickness leads to increasing slip between non-salt interbed material and the surrounding salt. At the same time, the roof-beam slip decreases slightly.

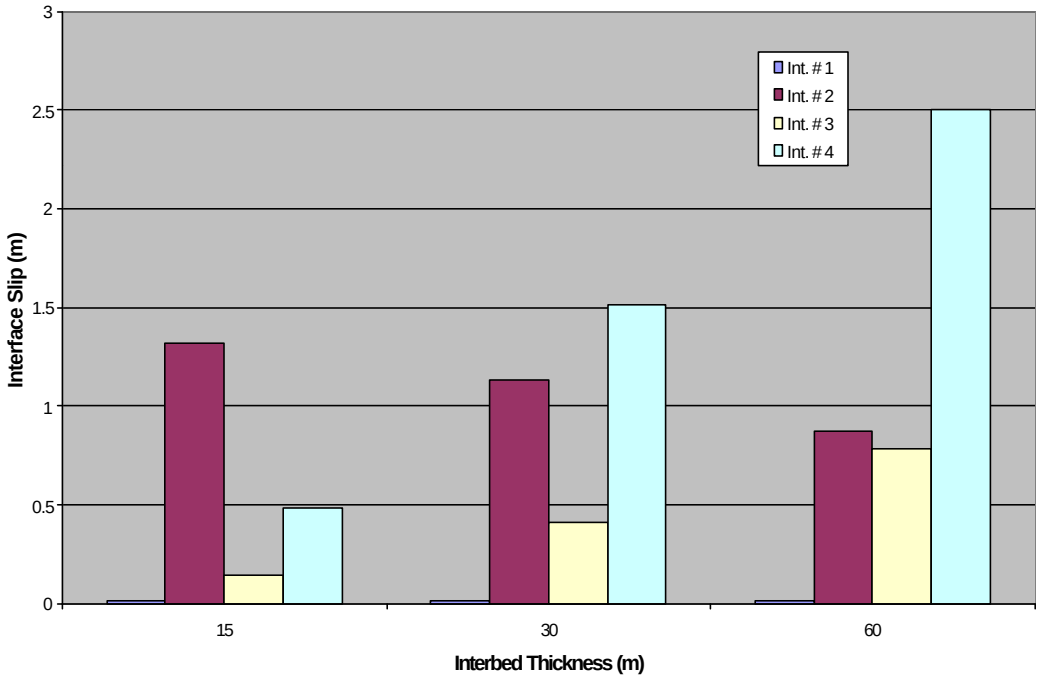

Figure 12. Influence of central non-salt interbed thickness on interface slip

3.5 Influence Roof Thickness on Deformation and Slip

To investigate the influence of roof thickness on deformation and slip, we consider variations in the thickness of the salt roof beam at the top of the cavern (simulations 1,5,6) and variations in the thickness of the non-salt interbed in the roof beam (simulations 1,2,3). Figure 13 presents simulation results as the salt roof beam is varied from 10m to 50m. Increasing salt roof beam thickness is seen to decrease the propensity for roof beam interface slip. Figure 14 presents simulation results as the overlying non-salt roof beam is varied from 5m to 20m. This appears to have no influence on slip and deformation. In retrospect, it may have been more illustrative to evaluate a non-salt interbed contained within a salt roof beam, rather than between the salt and overburden.

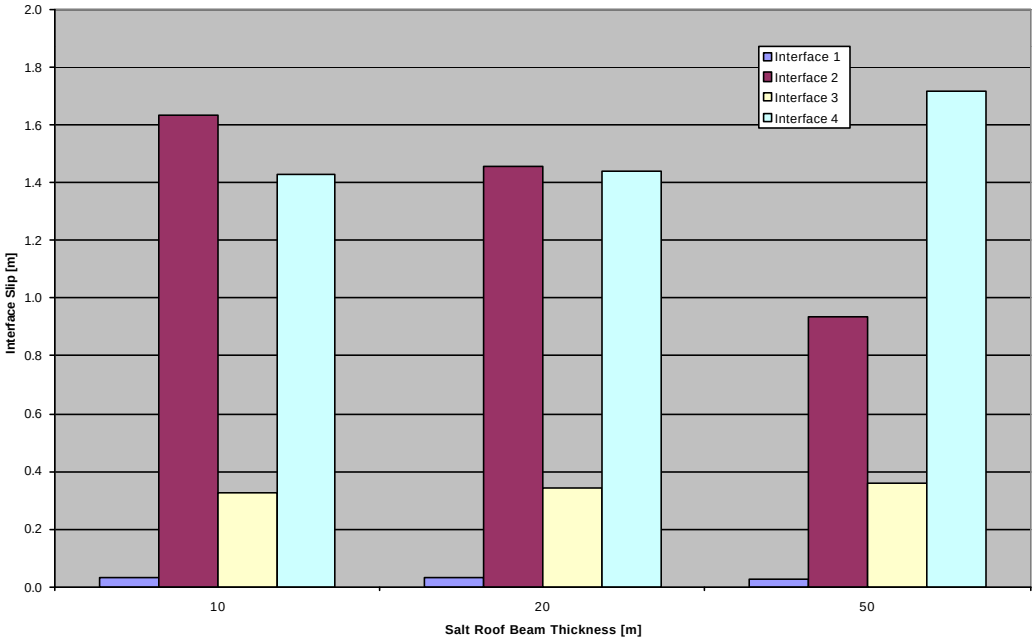

Figure 13. Influence of salt roof beam thickness on interface slip

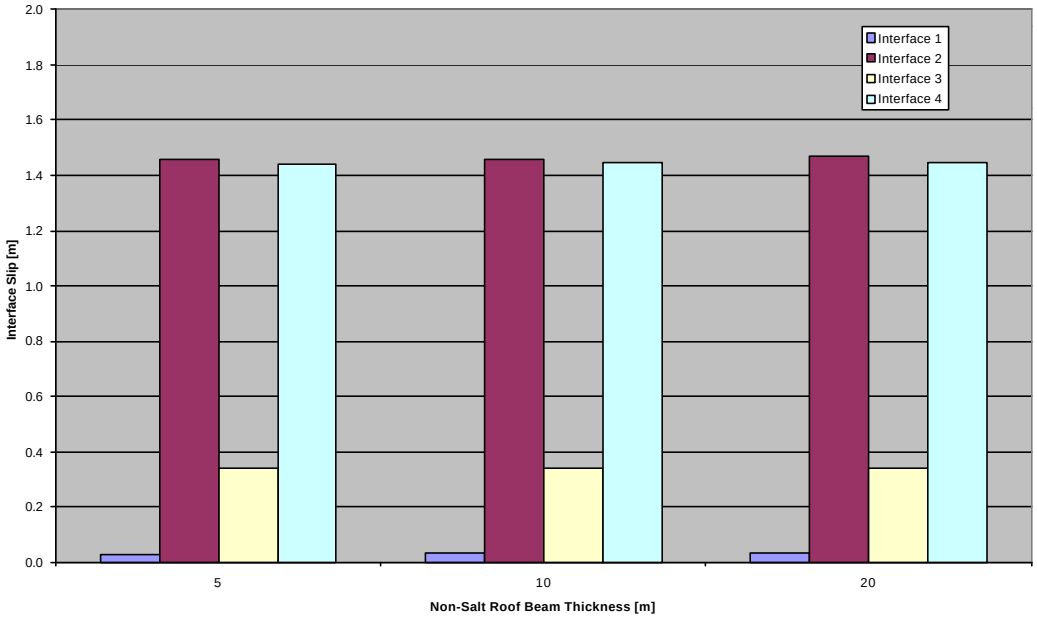

Figure 14. Influence of non-salt roof beam thickness on interface slip

3.6 Modeling Summary and Discussion

For the GRI project Terralog completed eleven geomechanical simulations to investigate cavern deformation and bedding plane slip for varying cavern geometry, interbed properties, and roof beam properties. In general, heterogeneous material layers across the cavern height and in the roof beam influence cavern integrity in three ways: first, by providing locations at which horizontal stresses (and related hydraulic fracture pressure) are lower than surrounding salt stresses; second, by providing interface locations along the cavern height for potential bedding plane slip and horizontal gas migration; and third, by providing interface locations in the cavern roof area for potential bedding plane slip, leading to increased risks for well casing damage and for roof caving.

A limited number of simulations have been completed to investigate and illustrate the relative influences of cavern height to diameter ratio, central non-salt interbed number and thickness, and salt and non-salt roof-beam thickness on cavern deformation and bedding plane slip. These initial simulations support the following observations:

1. Non-salt interbeds across the cavern height provide areas of lower horizontal stress and subsequent lower resistance to hydraulic fracturing;
2. Bedding plane slip in general becomes more severe during pressure depletion cycles, when the difference in pressure between internal cavern pressure and stresses in the surrounding salt is most severe;
3. Caverns with height to diameter ratio less than one produce increased risk for roof beam interface slip, and therefore increased risk for well casing damage and roof caving;
4. Caverns with height to diameter ratio greater than one, which also include non-salt interbeds along the height, provide increased risk for interface slip along those beds;
5. Additional non-salt interbeds near the center of the cavern do not significantly influence the bedding plane slip in the roof interbed or in other non-salt interbeds near the cavern center. They merely seem to provide locations for additional slip;
6. Increased non-salt interbed thickness leads to increased slip with the adjacent salt; and
7. Increased salt beam thickness reduces risks for roof beam interface slip.

Some of these observations are consistent with trends expected from the analytical investigations discussed in Section 4. Other observations are less obvious from the analytical studies, and deserve greater scrutiny. The numerical investigations completed to date are limited in number, and should be expanded to better verify the trends noted and implications for cavern design and operations.

4. CONCLUSIONS

The general steps required to assess bedded cavern pressure limits may be summarized as follows:

1. Evaluate the geologic setting, including detailed stratigraphy, lithology, and number and type of interbeds;
2. Determine the mechanical properties of the salt and non-salt interbed materials;
3. Determine the *in situ* stresses and fracture pressures for individual formations;
4. Evaluate fracture pressure variations after cavern development;
5. Evaluate stresses induced by pressure cycling with geomechanical modeling;
6. Compare stresses induced by pressure cycling with estimated *in situ* stresses and formation fracture pressures; and,
7. Evaluate bedding plane slip and potential impact on cavern integrity.

A geomechanical model, of the type described in this report, may then be assembled and applied to investigate cavern closure and formation interface shear arising from expansion and contraction of the cavern during pressure cycling. Input data for the model can be applied from the geologic review, the estimate of mechanical properties and the estimate of stresses determined in the previous steps. When there is uncertainty (as is often the case) in input data, it is useful to perform parametric simulations for a range of assumed properties.

The preliminary geomechanical review and simulation results should then be evaluated to answer the following questions:

- Does the proposed maximum cavern pressure exceed the estimated fracture pressure for the weakest lithology?
- Will pressure cycling induce bedding plane slip at the cavern boundaries? If so, how much slip and will that cause potential communication problems (for example with nearby faults or other caverns?
- Are the shear stresses induced in the overburden enough to cause potential faulting and bedding plane slip, leading to possible roof caving or well casing damage?

In summary, cavern development and operation in thin bedded salt provides additional challenges over conventional domal salt cavern operations. The challenges are related to the heterogeneous material properties, the resulting differences in fracture pressure, and the potential for bedding plane slip across the cavern height (leading to gas migration risk) and within the roof and caprock (leading to roof caving and well shear damage risk). Notwithstanding these challenges, however, appropriate geologic characterization and geomechanical assessment efforts can be applied to safely develop and operate caverns in bedded salt formations.

5. REFERENCES

American Gas Association (AGA), 1998 Survey of Underground Storage of Natural Gas in the United States and Canada.

API, 1994, "Design of Solution-Mined Underground Storage Practices," API Recommended Practice 1114, American Petroleum Institute, Washington, DC, June.

Bruno, M.S. (2001): Geomechanical analysis and decision analysis for mitigating compaction related casing damage, SPE 71695 to be presented the SPE Ann. Tech. Conf, New Orleans, Sept. 30 – Oct. 3rd, 2001.

Bruno, M.S., Dewolf, G., and Foh, S. (2000): Geomechanical analysis and decision analysis for delta pressure operations in gas storage reservoirs, Proc. AGA Operations Conf., Denver, CO, May 7-9.

CSA - Canadian Standards Association, 1993. "Storage of Hydrocarbons in Underground Formations — Oil and Gas Industry Systems and Materials," Standard Z341-93, Canadian Standards Association, Rexdale, Ontario, Canada, July.

CSA - Canadian Standards Association, 1998. Code Z341-98 Storage of Hydrocarbons in Underground Formations

IOGCC, 1995, "Natural Gas Storage in Salt Caverns - A Guide for State Regulators," Interstate Oil and Gas Compact Commission, Oklahoma City, OK, October.

Johnson, K.S. and Gonzales, S., 1978. Salt Deposits in the United States and RegionalGeological Characteristics Important for Storage of Radioactive Wastes. Office of Waste Isolation, Union Carbide Corp., US Dept of Energy, Y/OW1/SUB-7414/1, 188 pp.

Neal, J.T. and Magorian, T.R., 1995. Geological Site Characterization Requirements for Storage and Mining is Salt. Proceedings Solution Mining Research Institute Spring Meeting, New Orleans LA, 19 pages.